Diyala Journal of Engineering Sciences

ISSN 1999-8716
Printed in Iraq

First Engineering Scientific Conference
College of Engineering –University of Diyala
22-23 December 2010, pp. 26-39

NUMERICAL SIMULATION OF THE LAMINAR FLOW OF NON-NEWTONIAN FLUID THROUGH A DISK-TYPE PROSTHETIC HEART VALVE

Tazyukov, F. Kh. and Khalaf, H.A.
Kazan State Technological University, Kazan, Russia.

ABSTRACT:-This work presents the numerical simulation of the laminar flow of Non-Newtonian fluid in a planar channel, which includes locking structure, consisting of the support ring and movable valve. Investigated characteristic of fluid flow in valve, fitted with an artificial valve, as well as the flow various emulsions in channels containing locking valves. As the rheological constitutive relation, the model of a Generalized Newtonian Fluid, predicts the effect of anomaly viscosity. The governed equations that describe the flow were integrated by the Finite Volumes Method, using SIMPLE algorithm. The mesh is structured, with rectangular volumes. Several boundary conditions were explored, being the more realistic results obtained by prescribing the inlet velocity field and atmospheric pressure at the exit. Stream function, mean axial velocity profile, normal and wall shear stresses distributions in the flow field surrounding the prosthetic valve are computed for various values of Reynolds numbers (Re=30, 60 and 90).

Keywords: laminar flow, Non-Newtonian Fluid, artificial valve, planar channel, Finite Volume Method, SIMPLE algorithm.

1. INTRODUCTION

In the recent years, to determine regions of high fluid stress and separated flow in the vicinity of prosthetic heart valves and to improve upon existing valve designs computational fluid dynamics techniques have recently become popular, especially for physiological flows. The problems of thrombosis and haemolysis are directly related to the fluid dynamics of the artificial valves[(1),(2)]. Table 1 presents experimental data for the extent of damage to blood cells and endothelial cells that can be expected at various levels of shearing stress. The

experimental measurement of flow through prosthetic valves is often restricted in application only to certain regions of the flow field (e.g. the aortic wall) or limited due to probe size. This has been the experience of previous researchers in this field[3],[4]. Computational fluid dynamic techniques provide an entirely noninvasive method for obtaining quantitative data for velocity and stress distributions near prosthetic heart valves. Other advantages over physical simulators include immediacy and observability[2].

In this paper, we study the steady flow of Newtonian and Generalized Newtonian Fluids in a plane channel containing a fully open valve disc type for different values of Reynolds number (Fig.1). Conditions on the boundaries of the flow are no-slip condition at solid walls. Walls themselves are smooth and impermeable undeformable. At the inlet is given by the rate of inflow. In the exit section is given by the steady flow regime. On the channel axis of symmetry conditions are imposed. The relative sizes of the closing device shown in Fig. 2.

For the testing the following fluids are used, Newtonian, pseudoplastic (shear thinning) and dilatant (shear thickening). In the Fig. 3, the dependence of shear stress on the shear rate is shown[5], [6].

2. GOVERNING EQUATIONS AND SOLUTION TECHNIQUE

The problem here considered is the two-dimensional isothermal flow of an incompressible liquid. This flow is governed by the usual equations of continuity and motion, which can be written in vector form as:

$$\vec{\nabla} \cdot \vec{v} = 0 \qquad \ldots\ldots\ldots (1)$$

$$\rho \vec{v} \cdot \nabla \vec{v} = -\vec{\nabla} p + \vec{\nabla} \cdot \tilde{\tau} \qquad \ldots\ldots\ldots (2)$$

where $\vec{v}$ is the velocity vector, p the pressure, $\tilde{\tau}$ the extra stress tensor, ρ the density and $\vec{\nabla} = \vec{i}\,\partial/\partial x + \vec{j}\,\partial/\partial y$.

The constitutive equation that relates the non-Newtonian stresses with the velocity gradients is given by the Generalized Newtonian Model[6], [7]:

$$\tilde{\tau} = \eta\, \tilde{\dot{\gamma}} \qquad \ldots\ldots\ldots (3)$$

where $\tilde{\dot{\gamma}} = \vec{\nabla}\vec{v} + \vec{\nabla}\vec{v}^{T}$ is the rate-of-strain tensor and η the effective viscosity given by the power-law model by

$$\eta = m\left|\tilde{\dot{\gamma}}\right|^{n-1} \qquad \ldots\ldots\ldots (4)$$

In this equation, m and n are two empirical curve-fitting parameters and are known as the fluid consistency coefficient and the flow behaviour index respectively. For a shear-thinning fluid, the index may have any value between 0 and 1. The smaller the value of n, the greater is the degree of shear-thinning. For a shear-thickening fluid, the index n will be greater than unity. When n=1, equations (3) and (4) reduce to equation $\tilde{\tau} = \mu\,\tilde{\dot{\gamma}}$, where μ - is Newtonian viscosity which describes Newtonian fluid behaviour[5].

In this work, we will consider three different flow indexes that are respectively associated with shear-thinning (n=0.8), Newtonian (n=1.0) and shear-thickening fluids (n=1.2).

The approach Reynolds number (Re) for power-law fluids is defined as, $\mathrm{Re} = \rho(2H)^n u_{in}^{2-n}/m$, where H-is half of channel diameter and u_{in}- velocity at inlet of channel.

2.1. Discretization

In order to numerically solve the velocity and pressure fields, the equations (1)-(4) above were discretized by the finite volume method. The method involves integrating the continuity and momentum equations over a two-dimensional control volume on a staggered differential grid[8], as shown in Fig. 4.

In the staggered grid, the calculated domain is divided into control volumes defined by the dashed lines. The pressure is stored at the nodes marked (•) - the intersection of two unbroken grid lines and indicated by the capital letters P, W, E, N and S. The u-velocity components are stored at the east and the west cell faces of the control volume and indicated by the lower case letters e and w. The v-velocity components are located at the north and south cell faces of the control volume, which are indicated by the lower case letters n and s.

Δx is the sub-interval of the calculated length. Δy is the sub-interval of the calculated depth.

After discretization, the discretized continuity equation becomes:

$$\left[(\rho u)_e - (\rho u)_w\right]\Delta y + \left[(\rho v)_s - (\rho v)_n\right]\Delta x = 0 \qquad (5)$$

and the discretized u-momentum equation becomes

$$a_e^{(u)} u_e = \sum a_{nb}^{(u)} u_{nb} + b^{(u)} + (P_P - P_E)\Delta y \qquad (6)$$

with : $a_e^{(u)} = \frac{\rho_e^o \Delta x \Delta y}{\Delta t} + a_E^{(u)} + a_W^{(u)} + a_S^{(u)} + a_N^{(u)}$, $b^{(u)} = u_e^o \frac{\rho_e^o \Delta x \Delta y}{\Delta t}$

and the discretized y-momentum equation can be written as:

$$a_e^{(v)} u_e = \sum a_{nb}^{(v)} u_{nb} + b^{(v)} + \left(P_N - P_P\right)\Delta x \qquad (7)$$

with : $a_e^{(v)} = \frac{\rho_n^o \Delta x \Delta y}{\Delta t} + a_E^{(v)} + a_W^{(v)} + a_S^{(v)} + a_N^{(v)}$, $b^{(v)} = v_e^o \frac{\rho_n^o \Delta x \Delta y}{\Delta t}$

where : ρ_e^o , ρ_n^o , u_e^o and v_n^o refer to the known values at time t, while all other values are the unknown values at time t+Δt. The coefficients with superscripts (u) and (v) refer to the coefficients corresponding to u and v, respectively. $a_{nb}^{(u)}$, $a_{nb}^{(v)}$ refer to the neighbour coefficients $a_E^{(u)}$, $a_W^{(u)}$, $a_N^{(u)}$, $a_S^{(u)}$, $a_E^{(v)}$, $a_W^{(v)}$, $a_N^{(v)}$ and $a_S^{(v)}$ which account for the combined convection-diffusion influence at the control-volume faces of u-cell and v-cell, respectively.

The values of these coefficients are obtained on the basis of the power-1aw scheme[8]. The velocity components u_{ab} and v_{ab} are those at the neighbouring nodes outside the control volume P_E, P_W, P_N and P_S refer to the pressure at the east, the west, the north and the south faces of the control volume, respectively.

2.2. Numerical Procedure

To solve equations (5)-(7), the SIMPLE algorithm[8, 9], which is essentially a guess-and-correct procedure for the calculation of pressure on the staggered grid introduced above, is applied. To initiate the SIMPLE calculation process, a pressure field p* is guessed. The discretised momentum equations (6) and (7) are solved using the guessed pressure field to yield velocity components u* and v* as follows:

$$a_e^{(u)} u_e^* = \sum a_{nb}^{(u)} u_{nb}^* + b^{(u)} + \left(P_P^* - P_E^*\right)\Delta y \qquad (8)$$

$$a_n^{(v)} v_n^* = \sum a_{nb}^{(v)} v_{nb}^* + b^{(v)} + \left(P_N^* - P_P^*\right)\Delta x \qquad (9)$$

Defining the correction p' as the difference between the correct pressure field p and the guessed pressure field p*, so that:

$$p = p^* + p' \qquad (10)$$

Similarly defining the velocity correction u' and v' to relate the correct velocities u and v to the guessed velocities u* and v*:

$$u = u^* + u' \qquad (11)$$

$$v = v^* + v' \qquad (12)$$

By subtracting equations (8) and (9) from (6) and (7) respectively, it gives

$$a_e^{(u)}\left(u_e - u_e^*\right) = \sum a_{nb}^{(u)}\left(u_{nb} - u_{nb}^*\right) + \left[\left(P_P - P_P^*\right) - \left(P_E - P_E^*\right)\right]\Delta y \quad (13)$$

$$a_n^{(v)}\left(v_n - v_n^*\right) = \sum a_{nb}^{(v)}\left(v_{nb} - v_{nb}^*\right) + \left[\left(P_N - P_N^*\right) - \left(P_P - P_P^*\right)\right]\Delta x \quad (14)$$

Using the correction formulae (10)-(12), the equations (13) and (14) can be written as follows:

$$a_e^{(u)}u_e' = \sum a_{nb}^{(u)}u_{nb}' + \left(P_P' - P_E'\right)\Delta y \quad (15)$$

$$a_e^{(v)}v_e' = \sum a_{nb}^{(v)}v_{nb}' + \left(P_N' - P_P'\right)\Delta x \quad (16)$$

In the SIMPLE algorithm, the terms $\sum a_{nb}^{(u)}u_{nb}'$ and $\sum a_{nb}^{(v)}v_{nb}'$ are dropped, to simplify equations (15) and (16) for velocity corrections. Therefore, we obtain:

$$u_e' = \frac{\Delta y}{a_e^{(u)}}\left(P_P' - P_E'\right) \quad (17)$$

$$v_n' = \frac{\Delta x}{a_n^{(v)}}\left(P_N' - P_P'\right) \quad (18)$$

Substituting equations (17) and (18) into (11) and (12) gives:

$$u_e = u_e^* + \frac{\Delta y}{a_e^{(u)}}\left(P_P' - P_E'\right) \quad (19)$$

$$v_n = v_n^* + \frac{\Delta x}{a_n^{(v)}}\left(P_N' - P_P'\right) \quad (20)$$

Similarly we have:

$$u_w = u_w^* + \frac{\Delta y}{a_w^{(u)}}\left(P_W' - P_P'\right) \quad (21)$$

$$v_s = v_s^* + \frac{\Delta x}{a_s^{(v)}}\left(P_P' - P_S'\right) \quad (22)$$

Substituting equations (19)-(22) into the discretised continuity equation (5), we draw the pressure-correction equation which plays an important part in the SIMPLE algorithm as follows:

$$a_p P_P' = a_E P_E' + a_W P_W' + a_N P_N' + a_S P_S' + \left[\left(\rho u^*\right)_w - \left(\rho u^*\right)_E\right]\Delta y + \left[\left(\rho v^*\right)_n - \left(\rho v^*\right)_s\right]\Delta x \quad (23)$$

where : $a_p = a_E + a_W + a_N + a_S$

$$a_E = \rho_e \frac{(\Delta y)^2}{a_e};\ a_W = \rho_W \frac{(\Delta y)^2}{a_w}\ ;\ a_N = \rho_N \frac{(\Delta x)^2}{a_n}\ ;\ a_S = \rho_S \frac{(\Delta x)^2}{a_s}$$

The procedure of the SIMPLE algorithm is summarized Fig.5.

In performing the SIMPLE algorithm to solve the velocities, the TDMA (Tri-Diagonal Matrix Algorithm) or Thomas' algorithm, which has become almost standard for the treatment of tridiagonal systems of equations[9], is employed by line-by-line method.

To solve a general two-dimensional discretised equation with a form such as:

$$a_p\phi_p = a_E\phi_E + a_W\phi_W + a_N\phi_N + a_S\phi_S + b \qquad (24)$$

where

$$a_E = D_e A(|P_e|) + [[-F_e, 0]] \quad , \quad a_W = D_w A(|P_w|) + [[F_w, 0]]$$

$$a_N = D_n A(|P_n|) + [[-F_n, 0]] \quad , \quad a_S = D_s A(|P_s|) + [[-F_s, 0]]$$

$$a_P^0 = \frac{\rho_P^0 \Delta x \Delta y}{\Delta t} \ , \ b = S_c \Delta x \Delta y + a_P^0 \phi_P^0 \ , \ a_p = a_E + a_W + a_N + a_S + a_P^0 - S_P \Delta x \Delta y$$

Here ρ_P^0 and ϕ_P^0 refer to the known values at time t, while all other values (ϕ_p, ϕ_E , ϕ_W , ϕ_N ϕ_S , and so on).

The flow rates F_e, F_w , F_n and F_s , and the corresponding conductances are define by :

$$F_e = (\rho u)_e \Delta y \quad , \quad F_w = (\rho u)_w \Delta y \quad , \quad F_n = (\rho v)_n \Delta x \quad , \quad F_s = (\rho v)_s \Delta x \ ,$$

$$D_e = \Gamma_e \Delta y / (\delta x)_e \ , \ D_w = \Gamma_w \Delta y / (\delta x)_w \ , \ D_n = \Gamma_n \Delta x / (\delta y)_n \ , \ D_s = \Gamma_s \Delta x / (\delta y)_s$$

and the Peclet numbers by

$$P_e = F_e / D_e \quad , \quad P_w = F_w / D_w \quad , \quad P_w = F_w / D_w \ , \ P_e = F_e / D_e$$

The function $A(|P|)$ in this work is power law scheme, for which

$$A(|P|) = [[0, (1 - 0.1|P|)^5]] \qquad (25)$$

2.3. TREATMENT OF IRREGULARLY SHAPED OBJECTIVE IN CALCULATION DOMAIN

We now describe the manner in which we treat arbitrary geometries by the blocking-off method [8]. This is done by blocking off some of the control volumes of the regular grid, so that the remaining inactive control volumes form the desired irregular domain. Example is shown in Fig.1, where the shaded areas denote the inactive control volumes. It is obvious that arbitrary geometries are approximated by a series of the rectangular grids.

Idea of the blocking-off operation consists of establishing known values of the relevant ϕ's in the inactive control volumes. Here is a simple way in which the desired values

can be obtained in the inactive control volumes by setting a large source term in the discretization equations. For example, setting S_c and S_p in eq. (24) for the internal grid points (i.e., in the solid interior) as

$$S_C = 10^{30}\phi_{p,desired} \ , \ S_P = -10^{30}$$

where 10^{30} denotes a number large enough to make the other terms in the discretization equation negligible. The consequence is that

$$S_C + S_P\phi_P \approx 0, \ \ \phi_P = -S_C / S_P = \phi_{p,desired}$$

Note that this procedure can be easily used to represent irregularly shaped objective in the calculation domain by inserting such the internal boundary conditions.

3. THE RESULTS OF SIMULATION

Fig.6 shows the distribution of stream function for a pseudoplastic with n=0.8, a Newtonian (n=1), and a dilatants fluid with n=1.2 at the same distance from the ring to the locking disk. The recirculation present differences in size: for the pseudoplastic case the vortex is rounder than for the Newtonian, and for the dilatant it is thinner. Also separated flow regions computed downstream and attached to the sewing ring and behind the disk occluder can be clearly seen from the stream function contours for Re=30, 60 and 90.

Fig.7 gives axial velocity profiles at various locations in the flow field at x=1, 2.5 and 4.5 for Re=30, 60 and 90. The presence and intensity of reverse flow downstream of the occlude can also be clearly seen from Fig.7 distortion of the axial velocity profiles occurred due to lateral flow around the valve, and the disturbances decreased in magnitude downstream of the occluder. Fig.8 gives normal stresses τ_{xx} , τ_{yy} and shear stress τ_{xy} for the flow of a Non-Newtonian fluid at x=1, 2.5 and 4.5 for Re= 90.

Most of the physiological fluids possess pseudoplastic properties, that is, decreasing viscosity with increasing shear stress. It can be seen that for pseudoplastic fluids, the region of circulating flow is much greater. Consequently, shear-thickening blood having a lower value of non-Newtonian index actively promotes the formation of various plaques (atheroma) in the blood vessels' walls (aortic wall). Thrombi formed around the disk may come off and damage the closure of the valve.

It is known[(1)] that the shear stresses on the walls of blood vessels also affects the formation of atheromas. There is evidence[(2)] that the formations of atherosclerotic plaques, mainly occurs near the walls which are subjected to high or low shear stresses. Fig.9 shows

the distribution of wall shear stress for different values of the non-Newtonian index. It is visible that the peaks of shear stress are formed near the lock disk on the walls of blood vessels[7].

It can be seen from Fig.9 that during the flow of pseudoplastic fluids (shear-thinning, $n<1$) on the walls of blood vessels, peak shear stress is not formed. Whereas for dilatant fluids (shear-thickening, $n>1$) the peak shear stress become significant.

4. CONCLUSIONS

In this paper a finite volume method for two dimensional incompressible laminar flow in a planar channel, which includes locking structure, consisting of the support ring and movable valve was described. The numerical results obtained by this method for Newtonian and non-Newtonian (shear thickening and shear thinning) fluid flows were presented. For the generalized Newtonian fluids the power-law model was used.

Numerical simulations were conducted for the influence of the anomaly of viscosity on the sizes of the separated flow (circulation region) in the channel, which includes locking structure, consisting of the support ring and movable valve, as well as the values of wall shear stress near the given type of closing/locking device. Found that the anomaly of viscosity significantly affects all flow characteristics, including the size of circulation region and the formation of the peaks of wall shear stress. Conducting numerical experiments may allow a better understanding of the work of closing/locking valves and reduce the negative effects that occur during the flow of fluids directly related to the size of circulating stream and the values of wall shear stress.

5. REFERENCES

1. Peskin C.S., (1982), "The Fluid Dynamics of Heart Valves: Experimental, Theoretical and Computational Methods", Ann. Rev. Fluid Mech., Vol.14, Pp.235-259.
2. Thalassoudis, K. and Mazumdar, J., (1984), "Mathematical Model for Turbulent Blood Flow through a Disk-type Prosthetic Heart Valve, Medical and Biological Engineering and Computing", Vol. 22, Pp.529-536.
3. Figliola, R.S. and Mueller, T.J., (1981), "On the Hemolytic and Thrombogenic Potential of Occluder Prosthetic Heart Valves from in Vitro Measurements", Ibid., 103, Pp.83-90.

4. Herkes, W.H. and Lloyd, J.R., (1981), "Experimental Measurements of the Flow-Induced Shear Stress Distribution in the Vicinity of Prosthetic Heart Valves". ASME J. Biomech. Eng., 103, Pp.267-274.
5. Chhabra, R.P. and Richardson, J.F., (1999), "Non-Newtonian Flow in the Process Industries", Biddles Ltd, Guildford and King's Lynn, Great Britain.
6. Robertson, A.M., Sequeira, A., and Kameneva, M.V. (2008), "Hemorheology. Hemodynamical Flows: Modeling, Analysis and Simulation", Galdi, G., Rannacher, R., Robertson, A.M. & Turek, S. (eds.) Birkhauser Verlag AG, Basel, Boston, Berlin.
7. Khalaf, H.A., Aliev, K.M. and Tazyukov, F. Kh., (2010), "Laminar Flow of Generalized Newtonian Fluid in a Channel Containing the Open Valve", Pp. 238-241, VII Workshop for young scientists and specialists;"Heat and Mass Transfer Problems and Hydrodynamics in Power Machine", 15-17 September 2010, Kazan-Russia.
8. Patankar, S.V., (1980), "Numerical Heat Transfer and Fluid Flow", Hemispher, New York.
9. Versteeg, H.K., and Malalasekera, W., (1995), "An Introduction to Computational Fluid Dynamics: The Finite Volume Method", Addison Wesley Longman, Ltd., Harlow, England.
10. Blackshear, P.L., (1972), "Hemolysis at Prosthetic Surfaces. In Chemistry of Biosurfaces", HAIR, M. L. (Ed.), Marcel Dekker, New York, Vol. 2, Pp.523-561.
11. Fry, D.L., (1968), "Acute Vascular Endothelial Changes Associated with Increased Blood Velocity Gradients". Circ. Res., 22, Pp.165-197.
12. Hung, T.C., Hochmuch, R.M., Joist, J.H. and Sutera, S.P., (1976), "Shear-Induced Aggregation and Lysis of Platelets", Trans. Am. Soc. Artif Intern. Organs, 22, Pp.285-290.
13. Hellums, J.D. and Brown, C.H. III, (1977), "Blood Cell Damage by Mechanical Forces. In Cardiovascular Fluid Dynamics", HWANG, N.H.C. and NORMANN, N.A. (Eds.), University Park Press, Baltimore, Pp.799-823.
14. Nevaril, C.G., Hellums, J.D., Alfrey, C.P.JR. and Lynch, E.C., (1969), "Physical Effects in Red Blood Cell Trauma", Am. Inst. Chem. Eng., 15, Pp.707-711.

Table (1): Effects of shear stress on blood cells and endothelial cells[2].

Shear stress, N/m^{-2}	Experimental observations
1-10	adhered red blood cells damaged[10]
≈40	endothelial cells damaged [11]
10-50	platelets damaged[12], [13]
≈95	endothelial cells erode away[11]
150-4000	damage to red blood cells in flow[10], [14]

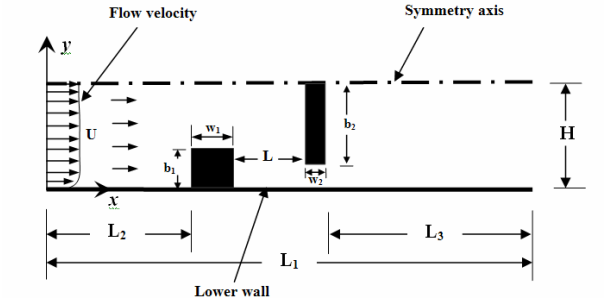

Fig. (1): Sketch of the contraction geometry.

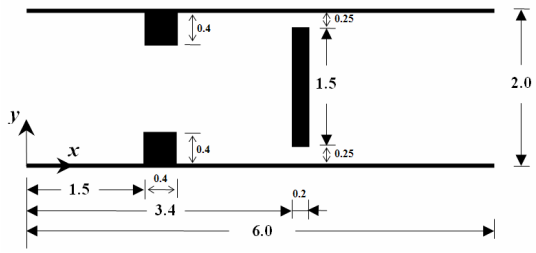

Fig.(2): Dimensions of the contraction geometry.

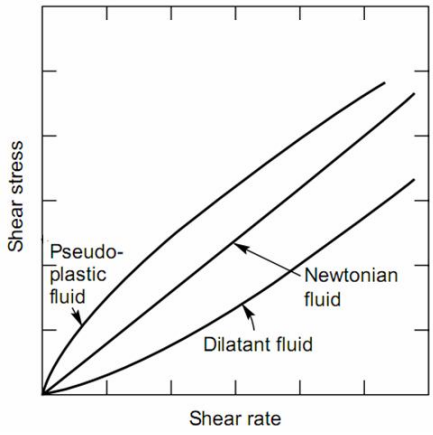

Fig. (3): Types of time-independent flow behaviour.

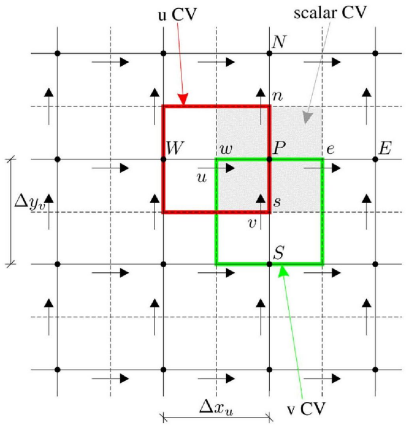

Fig.(4): Staggered grid describing a control volume with flow variables for two-dimensional situation.

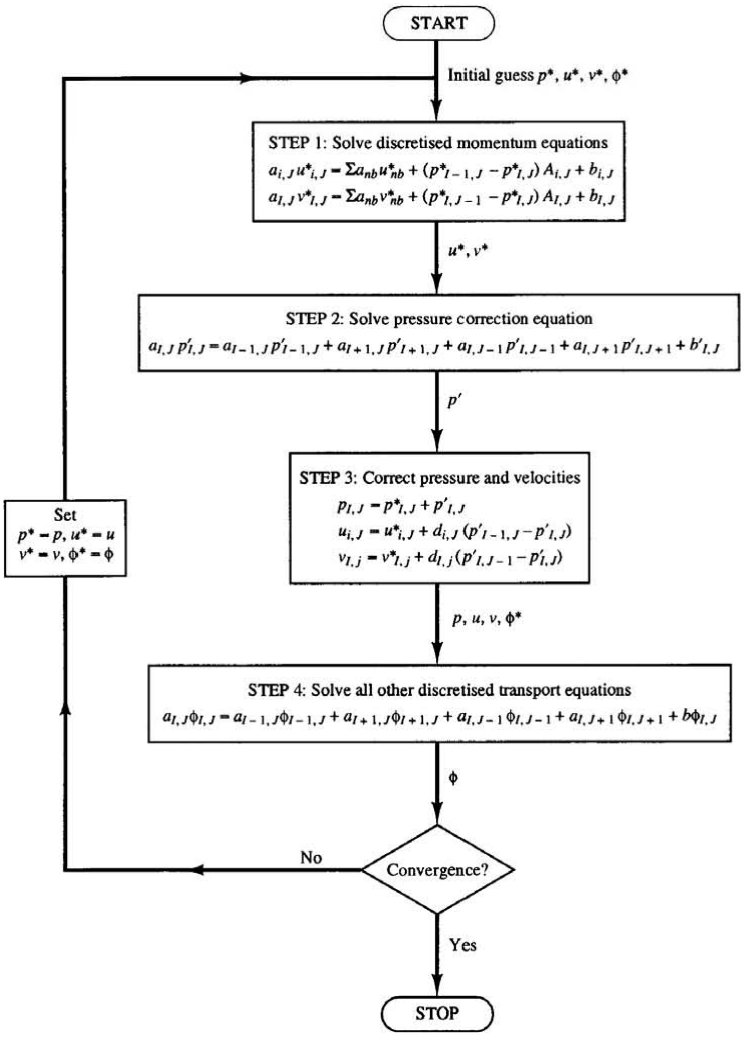

Fig. (5): SIMPLE Algorithm.

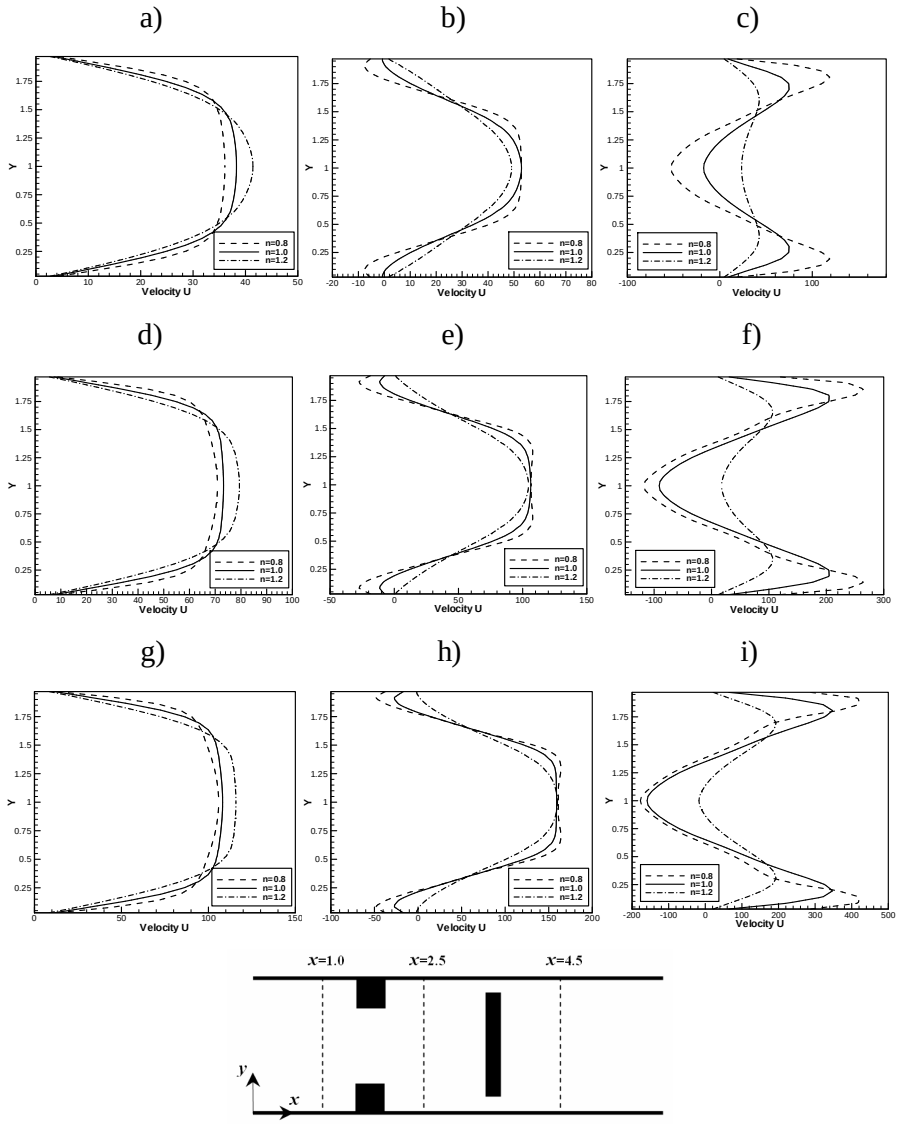

Fig.(7): Axial velocity profiles for the flow of a Non-Newtonian fluid. a) x=1.0 at Re=30 , b) x=2.5 at Re=30 , c) x=4.5 at Re=30 , d) x=1.0 at Re=60 , e) x=2.5 at Re=60 , f) x=4.5 at Re=60 , g) x=1.0 at Re=90 , h) x=2.5 at Re=90 and i) x=4.5 at Re=90.

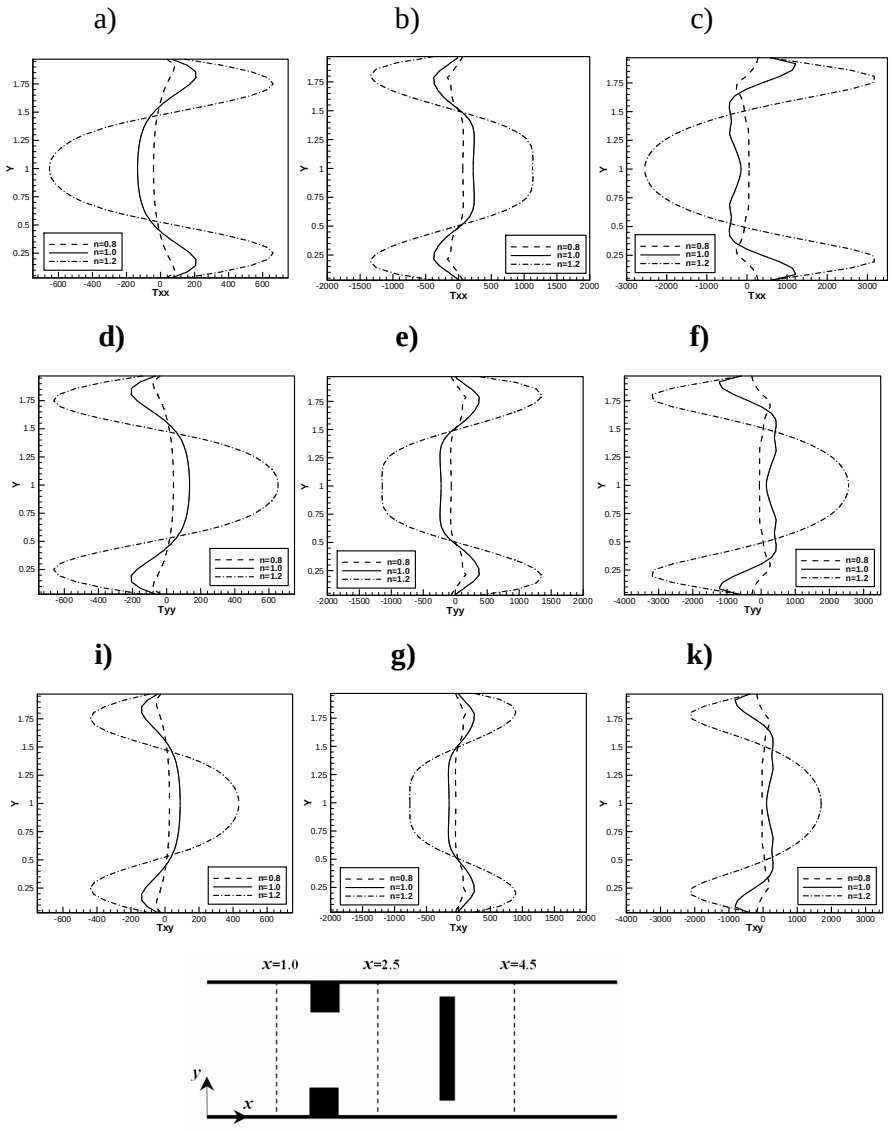

Fig.(8): Normal stresses τ_{xx}, τ_{yy} and shear stress τ_{xy} for the flow of a Non-Newtonian for Re=90. a) τ_{xx} at x=1, b) τ_{xx} at x=2.5, c) τ_{xx} at x=4.5, d) τ_{yy} at x=1, e) τ_{yy} at x=2.5, f) τ_{yy} at x=4.5, i) τ_{xy} at x=1, j) τ_{xy} at x=2.5 and k) τ_{xy} at x=4.5

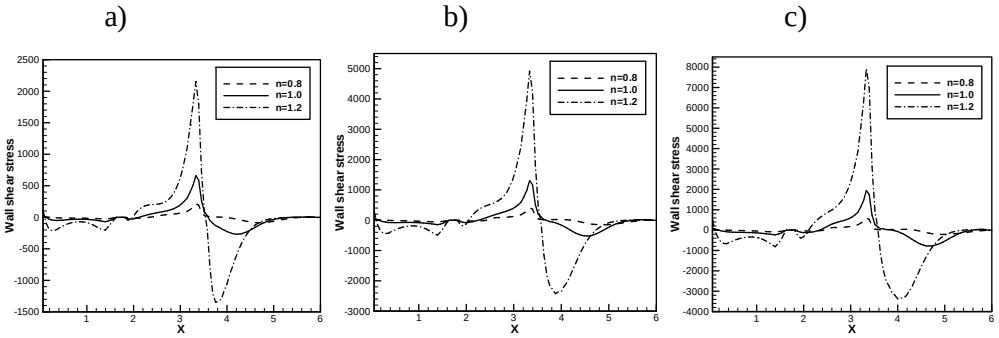

Fig.(9): Wall Shear Stress for the flow of a Non-Newtonian fluid.
a) Re=30 , b) Re=60 and c) Re=90.

المحاكاة العددية للتدفقِ الطباقيٍ للسوائلِ غيرِ النيوتونيةِ خلال صمام القلبِ الترقيعيٍ من نوعِ القرصَ

الدّكتور تازيكوف[1]، فاروق* و خلف[1] **، حسام علي
جامعة قازان التكنولوجية الحكومية ، قازان، روسيا

الخلاصة

العمل الحالي يعرض المحاكاة العددية للتدفق الطباقي للسوائل غير النيوتونية في قناة مستوية، التي تؤمن هيكلية القفل، والتي تتألف من حلقة ثابتة وصمام متحرك. فحُصت خصائص تدفق السائل في الصمام الاصطناعي، بالاضافة الى التدفق في قنوات مختلفة المستحلبات التي تحتوي على صمامات القفل. اما بالنسبة الى علاقة رهلوجيكل الجوهرية، فقد تم اخذ نموذج السائل النيوتوني المعمم، للتنبأ بتأثير اللزوجة. المعادلات التفاضلية التي تصف التدفق حُلت باستخدام طريقة الحجوم المنتهية، في بعدين، بأستخدام خوارزمية SIMPLE. خطوط الانسياب ومعدل السرعة الخطية وتوزيع الاجهادات العمودية والقص لمجال الجريان المحيط بالصمام، حسبت لقيم مختلفة من ارقام الرينولد (Re=30, 60 And 90)